Acta Pharmaceutica Sinica B 2021;11(4):989−1002

Chinese Pharmaceutical Association
Institute of Materia Medica, Chinese Academy of Medical Sciences

Acta Pharmaceutica Sinica B

www.elsevier.com/locate/apsb
www.sciencedirect.com

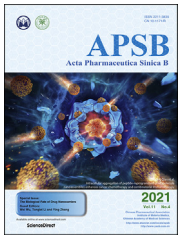

ORIGINAL ARTICLE

In vivo testing of mucus-permeating nanoparticles for oral insulin delivery using *Caenorhabditis elegans* as a model under hyperglycemic conditions

Ana L. Martínez-López[a], Carlos J. González-Navarro[b], Paula Aranaz[b], José L. Vizmanos[c,d], Juan M. Irache[a,*]

[a]*NANO-VAC Research Group, Department of Chemistry and Pharmaceutical Technology, School of Pharmacy and Nutrition, University of Navarra, Pamplona 31080, Spain*
[b]*Center for Nutrition Research, School of Pharmacy and Nutrition, University of Navarra, Pamplona 31080, Spain*
[c]*Department of Biochemistry & Genetics, School of Science, University of Navarra, Pamplona 31080, Spain*
[d]*Navarra Institute for Health Research (IdiSNA), Pamplona 31080, Spain*

Received 8 November 2020; received in revised form 18 December 2020; accepted 6 January 2021

KEY WORDS

Nanoparticles;
Oral delivery;
Mucus-permeating;
Biodistribution;
Insulin;
Caenorhabditis elegans;
ROS;

Abstract The aim was to evaluate the potential of mucus-permeating nanoparticles for the oral administration of insulin. These nanocarriers, based on the coating of zein nanoparticles with a polymer conjugate containing PEG, displayed a size of 260 nm with a negative surface charge and an insulin payload of 77 μg/mg. In intestinal pig mucus, the diffusivity of these nanoparticles (PPA-NPs) was found to be 20-fold higher than bare nanoparticles (NPs). These results were in line with the biodistribution study in rats, in which NPs remained trapped in the mucus, whereas PPA-NPs were able to cross this layer and reach the epithelium surface. The therapeutic efficacy was evaluated in *Caenorhabditis elegans* grown under high glucose conditions. In this model, worms treated with insulin-loaded in PPA-NPs displayed a longer

Abbreviations: DAPI, 4′,6-diamidino-2-phenylindole; D_{eff}, effective diffusion coefficient; EDC, *N*-(3-di-methylaminopropyl)-*N*′-ethylcarbodiimide; FT-IR, Fourier transform infrared spectroscopy; FUdR, 5-fluoro-2′-deoxyuridine; GIT, gastrointestinal tract; H_2DCF-DA, 2,7′-dichlorodihydro fluorescein diacetate; ^{1}H NMR, ^{1}H nuclear magnetic resonance; HPLC, high-performance liquid chromatography; I, insulin; IIS, insulin/IGF-1 signaling; MSD, mean square displacement; NGM, nematode growth medium; NPs, nanoparticles; ORL, orlistat; PBST, phosphate-buffered saline with triton; PDI, polydispersity index; PEG, poly(ethylene glycol); PPA, PEG-poly(anhydride) conjugate; PPA-NPs, PEG-poly(anhydride)-coated zein nanoparticles; ROS, reactive oxygen species; SEM, scanning electron microscopy; SOD, superoxide dismutase; THF, tetrahydrofuran.

*Corresponding author. Tel.: +34948425600, fax: +34948425619.
E-mail address: jmirache@unav.es (Juan M. Irache).

Peer review under the responsibility of Chinese Pharmaceutical Association and Institute of Materia Medica, Chinese Academy of Medical Sciences.

https://doi.org/10.1016/j.apsb.2021.02.020

Lifespan;
Zein;
Epithelium

lifespan than those treated with insulin free or nanoencapsulated in NPs. This finding was associated with a significant reduction in the formation of reactive oxygen species (ROS) as well as an important decrease in the glucose and fat content in worms. These effects would be related with the mucus-permeating ability of PPA-NPs that would facilitate the passage through the intestinal peritrophic-like dense layer of worms (similar to mucus) and, thus, the absorption of insulin.

1. Introduction

Protein and peptide-based drugs are the current therapy for many diseases and the axis of the future in pharmaceutical research. On the other hand, although the oral route is the most common method of drug administration and the most accepted by patients, the adequate formulation of drugs based on proteins and peptides remains a great challenge. In general, pre-systemic degradation, low diffusion rate across the mucus barrier and poor intestinal permeability are the main limitations associated with the oral delivery of these biotherapeutics[1,2]. In recent years, various strategies have been proposed and evaluated to overcome these drawbacks and, thus, improve the oral bioavailability of these drugs. Among others, these strategies were based on the use of specific excipients (*e.g.*, absorption enhancers)[1,3], enzyme inhibitors[4], liposomes[5,6] and polymer nanoparticles[7,8].

In this sense, increasing effort has been performed in the application of nanoparticles as delivery agents for oral administration of proteins; particularly for (or using as a model) insulin. In fact, the oral delivery of insulin may significantly improve the quality of life of patients routinely treated by the subcutaneous route. Apart from the high adherence to oral treatment by the patient, oral insulin would minimize peripheral hyperinsulinemia and other adverse effects (*i.e.*, possible hypoglycemia and weight gain) associated with the conventional subcutaneous treatments[9]. Thus, the encapsulation of insulin in nanoparticles based on non-toxic and biodegradable polymers has provided a promising approach by providing adequate protection against its physico-chemical and enzymatic degradation in the gastrointestinal tract (GIT)[10]. However, in some cases, these nanoparticles have shown a limited efficacy due to their interaction with mucins and other components of the protective mucus layer that lines the epithelium. This mucoadhesive phenomenon of polymeric nanoparticles may be of interest for increasing their residence time in the intestine and facilitate the controlled release and absorption of other small drugs (particularly with a lipophilic character)[11]. However, in the specific case of protein or peptides, the trapping of nanoparticles in the mucus layer would facilitate the inactivation and degradation of the therapeutic compound by the digestive enzymes faraway of the absorptive membrane.

One strategy to minimize this problem and increase the probability of nanoparticles to reach the epithelium would be the modification of their surface with hydrophilic compounds. This modification would produce an effective shield capable of avoiding the mucoadhesive interactions. To do this, different compounds and excipients have been proposed, including poly (ethylene glycol) or PEG[12,13] or thiamine[14].

On the other hand, the use of simple organisms to evaluate the fate[15] and efficacy[16] of nanoparticles is gaining attention as preliminary *in vivo* proof-of-concept assays prior to experimentation with mammals. In this line, *Caenorhabditis elegans*, an invertebrate animal model, provides some very versatile tools that allow modeling complex human diseases (*e.g.*, diabetes and Parkinson's disease), which cannot be easily reproduced *in vitro* in cellular models[17]. *C. elegans* has a short life-cycle and lifespan, transparent body, ease of culture, and well-established genetic pathways. Indeed, the insulin signaling pathway is highly conserved in *C. elegans* and mammals, being the primary pathway that regulates glucose and, particularly, fat metabolism[18]. Recently, *C. elegans* has been used as an alternative animal model for initial screening and evaluation of the oral drug delivery *via* nanocarriers, due to its resemblances to the mammalian intestinal barrier[19]. In particular, the intestinal microenvironment of the worm is integrated by a variety of digestive enzymes and pH ranges from pH 6, in the anterior pharynx, to pH 3.6 in the posterior intestine[20]. Besides, the intestinal lumen remains separate from the microvilli by a peritrophic-like membrane, glycocalyx, which protects the intestinal cells against mechanical injury, pathogens, and foreign materials[21]. Finally, the mechanisms of transport of biomolecules across the gastrointestinal barrier are also highly conserved, including the presence of tight junctions and efflux pumps such as P-glycoproteins[20].

The aim of this work was to explore the potential of mucus-permeating nanoparticles, based on the coating of zein nanoparticles (NPs) with a polymer conjugate containing PEG, as carriers for the oral delivery of insulin. Zein, the main storage protein in corn, has a GRAS status and can be easily transformed into nanoparticles with a significant ability to load biomacromolecules without compromising their integrity and activity[22]. However, zein NPs have important mucoadhesive properties[23,24] that limit their capability to reach the absorptive epithelium in which release the cargo. In order to solve this drawback and, thus, facilitate their passage through the protective mucus layer lining the epithelium, the zein nanoparticles were coated with a polymer conjugate obtained by the covalent binding of PEG 2000 to the anhydride groups of Gantrez®AN. The resulting nanocarriers were characterized and their biodistribution and efficacy evaluated in rats and *C. elegans*, respectively.

2. Materials and methods

2.1. Materials

Zein, human insulin, lysine, Nile red, orlistat, glucose, mannitol, isopropanol, sodium azide, tripton X-100, agarose, 5-fluoro-2′-

deoxyuridine (FUdR, 98%), *N*-(3-di-methylaminopropyl)-*N*′-ethylcarbodiimide (EDC), tetrahydrofuran (THF), deuterated dimethylsulphoxide (DMSO, 99.99% in deuterium), Rose Bengal salt and 2,7′-dichlorodihydro fluorescein diacetate (H_2DCF-DA) were purchased from Sigma−Aldrich (St. Louis, MO, USA). Gantrez® AN 119 or poly (anhydride) (MW of 97.7 kDa) was a gift from Ashland Inc (Covington, KY, USA). Poly (ethylene glycol) 2000 (PEG) was provided by Fluka (Buchs, Switzerland). Lumogen®F Red was provided by BASF (Ludwigshafen, Germany). BCA Protein Assay Kit and Gibco®PBS phosphate-buffered saline were provided by Thermo Fisher Scientific (Waltham, MA, USA). 4′,6-Diamidino-2-phenylindole (DAPI) was obtained from Biotium Inc (Fremont, CA) and O.C.T.™ Compound Tissue-Tek® was purchased from Sakura Finetek Europe BV (Alphen aan der Rijn, The Netherlands).

2.2. Synthesis and characterization of PEG-poly(anhydride) conjugate (PPA)

The PEG-poly (anhydride) conjugate was formed by the covalent bonding of PEG 2000 to the anhydride groups of Gantrez®AN, following a procedure previously described[25], with some modifications. Briefly, 100 mg poly (anhydride) and 25 mg EDC were dissolved in 6 mL of a mixture of acetone and THF (6:5, *v*/*v*) under moderate stirring and nitrogen atmosphere for 7 h in an ice bath. Then, 20 mg PEG 2000 (dispersed in 1 mL acetone) were added to the reaction mixture at 50 °C and stirred for 24 h in the dark. To remove the excess of reactants, the mixture was dialyzed in water for 12 h by a 3500 molecular weight cutoff (MWCO) dialysis membrane. Finally, the polymer resulting was frozen at −80 °C and freeze-dried in a Genesis 12 EL apparatus (SP VirTis, Warminster, PA, USA).

For the characterization, PPA was analyzed by infrared spectroscopy and ^{1}H NMR. The infrared spectra were recorded over the range of 600−4000 cm^{-1} (32 scans, 2 cm^{-1} resolution) on a Nicolet-FTIR Avatar 360 spectrometer (Thermo Fisher Scientific, Waltham, MA, USA), using an MKII Golden Gate ATR device with OMNIC E.S.P. software. ^{1}H NMR spectrum was recorded on a Bruker Advance DMX600 spectrophotometer (Bruker Optics Inc., Billerica, MA, USA) at a proton resonance frequency of 400 MHz. Samples were prepared in deuterated DMSO and the spectra were obtained at $n_s = 256$. The amount of PEG linked to the poly (anhydride) was estimated as described previously[26].

Elemental microanalyses of the synthesized conjugate were assessment in a LECO CHN-900 apparatus (Isomass Scientific Inc., Calgary, Canada). For this analysis, the samples (1 mg) were evaluated by triplicate, and the results were expressed as a percentage (%, *w*/*w*).

2.3. Preparation of insulin-loaded nanoparticles

Insulin was encapsulated in zein nanoparticles following a desolvation procedure[23]. The resulting nanoparticles were coated by incubation with the PPA conjugate and, after purification, dried in a Spray-drier apparatus. In brief, 1 mL of insulin solution (20 mg/mL) was added to 19 mL hydroalcoholic solution, containing 200 mg zein and 30 mg lysine, and stirred for 15 min. Then, 20 mL purified water was added and, after the formation of nanoparticles, 0.5 mL of a PPA conjugate solution in water (2%, *w*/*v*) was incorporated and incubated by stirring for 30 min. This mixture was concentrated and purified by ultrafiltration and, after the addition of mannitol as protectant, dried in a Büchi Mini Spray Drier B-290 (Büchi Labortechnik AG). The insulin-loaded into PPA-coated nanoparticles were named I-PPA-NPs.

Bare nanoparticles (I-NPs) were prepared in the same way but the absence of PPA. In a parallel, blank nanoparticles (used as controls) were also prepared but in the absence of insulin (PPA-NPs and NPs respectively).

2.4. Preparation of fluorescently labelled nanoparticles

Nanoparticles were fluorescently labelled by the encapsulation of Lumogen®F Red 305. For this purpose, 5 mg Lumogen®F Red were dissolved in the hydroalcoholic solution of zein and lysine. Nanoparticles were obtained and dried as described previously in Section 2.3. The stability of the marker in the nanoparticles was assessed as described previously[23].

2.5. Physico-chemical characterization of nanoparticles

2.5.1. Size, polydispersity index, zeta potential and yield

The diameter and polydispersity index (PDI) of spray-dried nanoparticles were measured by photon correlation spectroscopy (PCS) after dispersion in water (1/10). Zeta-potential of nanoparticles dispersed in KCl (0.1 mmol/L, pH 7.4) was determined by electrophoretic laser Doppler anemometry. All parameters were carried out in a Zetasizer analyser system (Brookhaven Instruments Corp., Holtsville, NY, USA).

The shape and surface morphological of the nanoparticles were examined by SEM. Briefly, nanoparticles were dispersed in water and centrifuged for 20 min at 28,000×*g*. The pellet was redispersed in water and mounted on SEM solid grid, dried and sputtered with a thin layer of gold using a Quorum Technologies Q150R S sputter-coated (Ontario, Canada) and analyzed using an ULTRA plus ZEISS field emission scanning electron microscope (FEG-SEM Zeiss Sigma 500, Jena, Germany). SEM images were obtained in secondary and backscattered electrons image mode.

The amount of protein transformed into nanoparticles was quantified by capillary electrophoresis-experion system (Bio-Rad Laboratories, Hercules, CA). For this, 5 mg of each formulation were dispersed in water and centrifuged for 20 min at 15,000×*g*. The pellets were dissolved in ethanol 75% and analyzed under reducing and non-reducing conditions according to the manufacturer's instructions (Experion Pro 260 Analysis kit; Bio-Rad Laboratories). For data analysis, Experion software version 3.10 (Bio-Rad Laboratories) was used. The yield for each formulation was calculated as the ratio between the quantity of the zein quantified in the pellet from samples and the total quantity of zein used for the preparation of nanoparticles.

2.5.2. Insulin-loaded quantification

The amount of insulin loaded in nanoparticles was quantified by HPLC as described previously[24] in an Agilent model 1100 series (Agilent Technologies, Waldbronn, Germany), coupled with a photodiode array detection system set at 220 nm. The separation of insulin was carried out at 27 °C on a TSKgel® G4000 column (7.8 mm × 30 cm; Tosoh Bioscience GmbH, Griesheim, Germany). The mobile phase consisted of a 0.3 mol/L NaCl solution in 0.05 mol/L phosphate buffer (pH 7) at a flow-rate of 0.8 mL/min. Standard curves in the range of 2−100 μg/mL ($R^2 \geq 0.999$) were prepared, and the samples were assayed in triplicate.

For analysis, nanoparticles, dispersed in water, were centrifuged and the pellet dissolved in ethanol 70% prior analysis. The payload was expressed as the amount of insulin (in μg) per mg of

nanoparticles. The encapsulation efficiency (EE, expressed in percentage) was calculated as the quotient between the amount of insulin quantified in the pellets (I_{loaded}) and the amount initially ($I_{initial}$) added for the preparation of nanoparticles as shown in Eq. (1):

$$EE\ (\%) = I_{loaded} / I_{initial} \times 100 \quad (1)$$

2.5.3. Surface hydrophobicity evaluation

The surface hydrophobicity of the different nanoparticles was evaluated by the Rose Bengal method[27]. Briefly, 500 µL of nanoparticle dispersions in water (from 0.04 to 4 mg/mL) were mixed with 1 mL of an aqueous solution of Rose Bengal (100 µg/mL). The samples were maintained for 30 min at 25 °C under constant shaking at 1500 rpm (Labnet VorTemp 56 EVC, Labnet International, Inc., Edison NJ, USA). Subsequently, the samples were centrifuged and the amount of Rose Bengal in the supernatants (unbound) was quantified at 548 nm in a microplate reader (BioTek PowerWave XS, BioTek Instruments Inc., Winooski, VT, USA). The absorption of the Rosa Bengal to nanoparticle surface (bound) was determined by the difference among the initial amount of the dye and amount or Rose Bengal unbound. The partitioning quotient (PQ) in Eq. (2) of each sample was plotted *versus* the total surface area (TSA). The slope of the line of the graph represents the hydrophobicity of the formulation. The higher the slope, the higher the hydrophobicity.

$$PQ = \text{Rose bengal bound} / \text{Rose bengal unbound} \quad (2)$$

2.6. Ex vivo mucus diffusion studies in porcine intestinal mucus

2.6.1. Collection and preparation of porcine mucus

The native porcine mucus was harvested from small intestine. The intestines were collected from the slaughterhouse and kept in ice-cold PBS (for a maximum period of 2 h) before the mucus collection. Intestine was cut into small portions that were opened to expose the lumen. Then, the exposed lumen was cleaned with PBS and the mucus collected using a spatula. The scraping was very gentle so as not to drag the epithelial tissue. The mucus obtained was transferred into 2 mL sample vials and stored at −80 °C.

2.6.2. Evaluation of the diffusion of nanoparticles in mucus by multiple particle tracking (MPT)

Nanoparticle diffusion through intestinal mucus was evaluated using the MPT technique, previously described[28,29]. In brief, 0.5 g of porcine intestinal mucus were tempered to 37 °C in imaging dishes with glass-bottom (MatTek Corp. Ashland, MA, USA). Then, a 25 µL aliquot of a suspension of fluorescently labelled nanoparticles (0.002%) was added and gentle shaking for 2 h (for efficient distribution of nanoparticles) before the video recording. Two-dimensional movies were captured at 30 frames/s for 10 s using a high-speed camera (Allied Vision Technologies, Stadtroda, Germany) mounted on a wide-field epifluorescence microscope equipped with a ×63 magnification oil immersion lens (Leica DM IRB, Wetzlar, Germany). At least 100 individual trajectories from each sample were tracked and analyzed in Fiji ImageJ software[30]. The MPT of each formulation was carried out in triplicate. The average of mean square displacement (MSD) in Eq. (3) and effective diffusion coefficient (D_{eff}) in Eq. (4) values were estimated for each nanoparticle as a function of time scale as previously described[28].

$$MSD = (X\Delta t)^2 + (Y\Delta t)^2 \quad (3)$$

$$D_{eff} = MSD / 4\Delta t \quad (4)$$

Finally, the diffusion of the nanoparticles in water ($D°$) at 37 °C was determined by the Stokes−Einstein equation (Eq. (5)) and compared with diffusion obtained in mucus (D_{eff}).

$$D° = kT / 6\pi\eta r \quad (5)$$

2.7. Biodistribution of nanoparticles in the gastrointestinal mucosa

These studies were performed as described previously[31] with minor modifications, after approval by the Ethical Committee of the University of Navarra following the European legislation on animal experiments (protocol 045−18).

The fate of nanoparticles in the gut of male Wistar rats (average weight 210 g; Harlan, Barcelona, Spain) was examined by fluorescence microscopy. For this purpose, 1 mL of a suspension of fluorescently labelled nanoparticles (25 mg/mL in water) was orally administered to fasting animals. Rats were euthanized 2 h after administration, and the guts were excised. Ileum sections of 1 cm were obtained, washed with PBS, and frozen at −80 °C after inclusion in Tissue-Tek® O.C.T.™ compound. Each portion was then cryosectioned into 5 µm thick, mounted to glass slides, and fixed with formaldehyde. The preparations were stained with DAPI to visualize cell nuclei of intestinal cells and preserve nanoparticle fluorescence. Images were taken on Zeiss AxioImager M1 fluorescence microscope (Zeiss, Oberkochen, Germany) and visualized with the software ZEN (Zeiss). As a control, an aqueous suspension of Lumogen®F Red 305 was administered.

2.8. In vivo evaluation of nanoparticles using C. elegans

2.8.1. Strains and cultivation

C. elegans N2 Bristol wild-type and *Escherichia coli* strain *OP50* were acquired from Caenorhabditis Genetics Center (CGC, University of Minnesota). *E. coli* OP50 was used as a food source. The worms were cultured on nematode growth medium (NGM) agar plates at 20 °C as described previously[32].

2.8.2. Treatment with nanoparticles

All assays were performed in triplicates in 6-well cell culture plates with 4 mL of glucose-supplemented (50 mmol/L) NGM per well. The effect of insulin (dissolved in water or loaded into nanoparticles) on *C. elegans* was evaluated at a concentration of 50 IU/mL in the NGM. Orlistat (6 µg/mL) was used as a positive control of fat reduction in *C. elegans*[33]. As controls, the same quantity of water was added to non-supplemented plates. After the addition of the treatments to the liquid-NGM-containing wells, they were mixed and allowed to solidify and dry in a dark environment. For all experiments, age-synchronized worms were obtained by treatment with alkaline hypochlorite solution (in which only eggs can survive), and eggs were let hatch for least 18 h in M9 buffer solution. Then, approximately 500 L1 larvae were

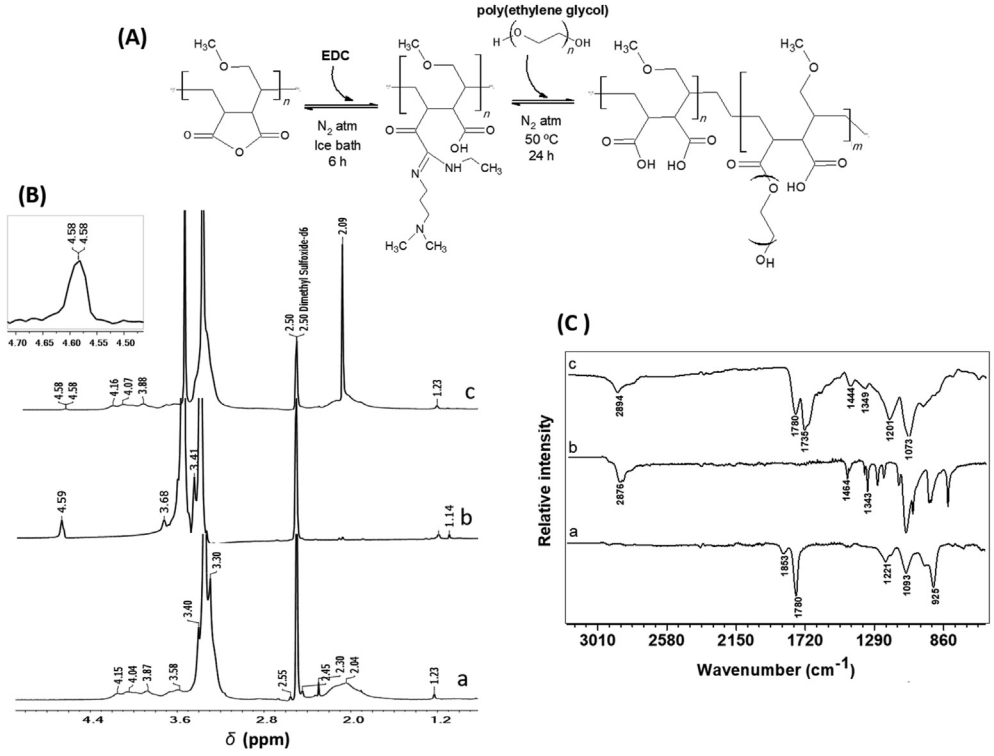

Figure 1 Characterization of PPA conjugate (A) Synthesis scheme of esterification reaction for the linkage of PEG2000 to Gantrez® AN (B) ^{1}H NMR spectra (DMSO-d_6) (C) FT-IR spectra of poly (anhydride) (a), PEG (b) and PPA conjugate (c).

transferred to plates and cultured to a definite age in each experiment.

2.8.3. *Nanoparticles intake*

To determine if worms consumed the nanoparticles, about 200 L4 worms were cultured on NGM plates with fluorescently labelled nanoparticles. After 2 h of treatment, worms were washed three times with M9 medium and then transferred onto slides provided with 2% agarose pads containing a 1% of sodium azide for anaesthetizing the worms. The fluorescently-loaded nanoparticles in the intestinal of worms were visualized on Zeiss Axio Imager M1 fluorescence microscope (Zeiss, Oberkochen, Germany).

2.8.4. *Glucose and SOD levels quantification*

Glucose levels in *C. elegans* were quantified as described before[34], with some modifications. Worms in the L1 stage were grown in NGM containing each treatment until the sixth day of adulthood. Then, 500 worms were harvested for each treatment and washed using phosphate-buffered saline with 0.01% Triton X-100 (PBST). Pelleted worms were then lysed by beat in homogenization buffer (PBST, 10 mmol/L NPs40) containing a protease inhibitor cocktail (complete™, Roche Diagnostics, Mannheim, Germany). Pelleted worms were then lysed by bead-beating in homogenization buffer (PBST, 10 mmol/L NPs40) containing a protease inhibitor cocktail (cOmplete™, Roche Diagnostics, Mannheim, Germany). The worms were homogenized at speed 10 for 2 × 2 min in a mini-Beadbeater (Biospec Products, Bartlesville, OK). Then, samples were centrifuged at 17,000×g for 5 min, and the supernatant sections were analyzed for glucose concentration (Accu-Check Aviva; Roche Diagnostics, Risch-Rotkreutz, Switzerland), protein concentration (BCA Protein Assay Kit) and superoxide dismutase (SOD) activity according to instructions of commercial Kit (BioVision Inc., Milpitas., CA).

Table 1 Elemental analysis and substitution degree (DS) of Gantrez® AN and the PEG conjugate (PPA).

Polymer	C (%)	H (%)	O (%)	N (%)	DS[a] (%)
Gantrez® AN	51.49	5.43	44.08	–	0
PPA	54.14	5.63	41.23	–	15.85 ± 1.30

[a]DS was determined by ^{1}H NMR spectroscopy and data represent mean ± SD (n = 3). –, Not applicable.

2.8.5. *Fat content quantification*

The fat content quantification in the worms was performed by the fixative-based Nile Red method[35]. Age-synchronized L1 worms were cultured in NGM containing each treatment until developing the L4 stage (48 h). At the L4 stage, the worms were collected from each treatment, washed with PBST and fixed in 40% isopropanol. Fixed worms were stained with a solution of Nile Red (3 μg/mL) for 30 min in dark conditions. After that, the worms were washed three times with PBST and mounted on a 2% agarose pad for microscopy evaluation. Fluorescent images of stained worms were taken on a Nikon SMZ18 stereomicroscope (Nikon Instruments Inc., Tokyo, Japan) equipped with a DS-FI1C refrigerated color digital camera and an epifluorescence system. The images were captured under a GFP filter (Ex 480−500, DM 505; BA 535−550) and analyzed using Fiji ImageJ software as previously described[38].

2.8.6. *Measurement of intracellular ROS*

Intracellular ROS in *C. elegans* was quantified using the molecular probe H_2DCF-DA as described previously[36]. For ROS detection, age-synchronized L1 worms were cultured in NGM containing

Table 2 Physico-chemical characteristics of empty (NPs and PPA-NPs) and insulin-loaded nanoparticles (I-NPs and I-PPA-NPs).

Nanoparticle	Mean size (nm)	PDI	Zeta potential (mV)	Yield (%)	Insulin loading (μg/mg NPs)
NPs	217 ± 5	0.17 ± 0.01	–45 ± 1	82 ± 3	–
I-NPs	253 ± 8	0.15 ± 0.04	–42 ± 2	81 ± 2	74.33 ± 2.68
PPA-NPs	225 ± 2	0.10 ± 0.05	–34 ± 2	84 ± 2	–
I-PPA-NPs	260 ± 4	0.18 ± 0.09	–32 ± 4	82 ± 1	76.68 ± 1.51

Data are expressed as mean ± SD; $n = 3$. –, Not applicable.

each treatment until the sixth day of adulthood. Then, 60 worms were harvested for each treatment, washed with PBST and resuspended in M9 buffer. Then fresh H_2DCF-DA was added to a final concentration of 50 μmol/L. Samples were analyzed in a black flat bottomed 96-well plate every 30 min for a total period of 180 min in a fluorescence spectrophotometer (TECAN, Männedorf, Switzerland) with an automatic microplate reader at excitation/emission wavelengths of 485 and 525 nm. At least three independent replicates were performed.

2.8.7. *Lifespan assays*

The lifespan assay was monitored at 20 °C under high glucose conditions[37]. Age-synchronized L1 worms were grown in NGM containing each treatment during the whole lifespan of the animals. At the L4 stage, the worms were collected and transferred to new treatment-NGM plates with 40 mmol/L of FUdR (prevent the growth of new worms). The pre-fertile period of adulthood was used as time zero ($t = 0$). The worms were regarded dead if they did not move after repeated mechanical stimuli. All experiments were carried out at least three times, and about 100 worms were used for each experiment.

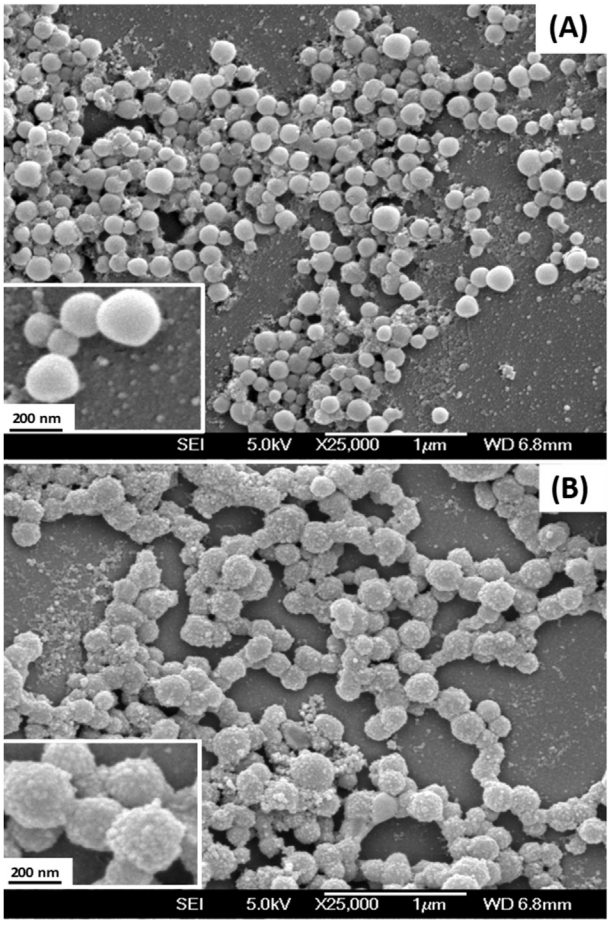

Figure 2 Scanning electron microscopy (SEM) images of spray-dried nanoparticles (A) Bare nanoparticles (NPs) (B) PPA-coated nanoparticles (PPA-NPs). A magnification of a section of each micrograph is shown in the left side.

2.8.8. *RNA extraction and quantitative PCR analysis*

Total RNA was extracted from L4 worms with TRIzol® RNA isolation reagent according to the manufacturer's instructions (Thermo Fisher Scientific, Paisley, UK). The RNA concentration and purity were examined at 260/280 nm using a NanoDrop spectrophotometer (Thermo-Fisher Scientific, Wilmington, DE). RNA purification and reverse transcription were achieved as described[38]. Quantitative RT-PCR was carried out in a CFX348 Touch™ Real-Time PCR detection system (BioRad Laboratories, Hercules, CA) using the TaqMan™ Universal PCR master mix and the corresponding specific probes from Life Technologies (TaqMan™ Gene Expression Assays, Applied Biosystems, CA). Gene expression levels were normalized compared to the expression of peroxisomal membrane protein-related gene (*pmp-3*) as housekeeping control[39]. Gene expression difference between insulin-treated and untreated samples was estimated using the relative quantification $2^{-\Delta\Delta Ct}$[40].

2.9. *Statistical analysis*

Means and standard errors were calculated for every data set. For body-fat reduction between treatments was evaluated by a hierarchical ANOVA test followed by multiple comparison (Fisher's, LSD) tests. For the rest of the parameters, statistical

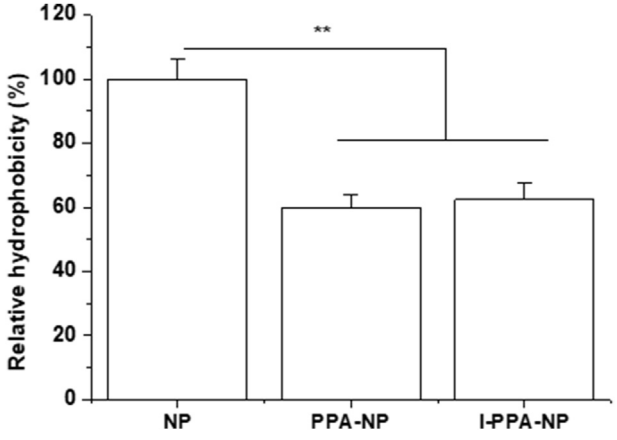

Figure 3 Relative hydrophobicity of the different formulations. Values are normalized to the hydrophobicity of bare nanoparticles (NPs). Data expressed as mean ± SD ($n = 3$). $^{**}P < 0.01$. PPA-NPs, PAA-coated nanoparticles; I-PPA-NPs, PPA-coated insulin-loaded nanoparticles.

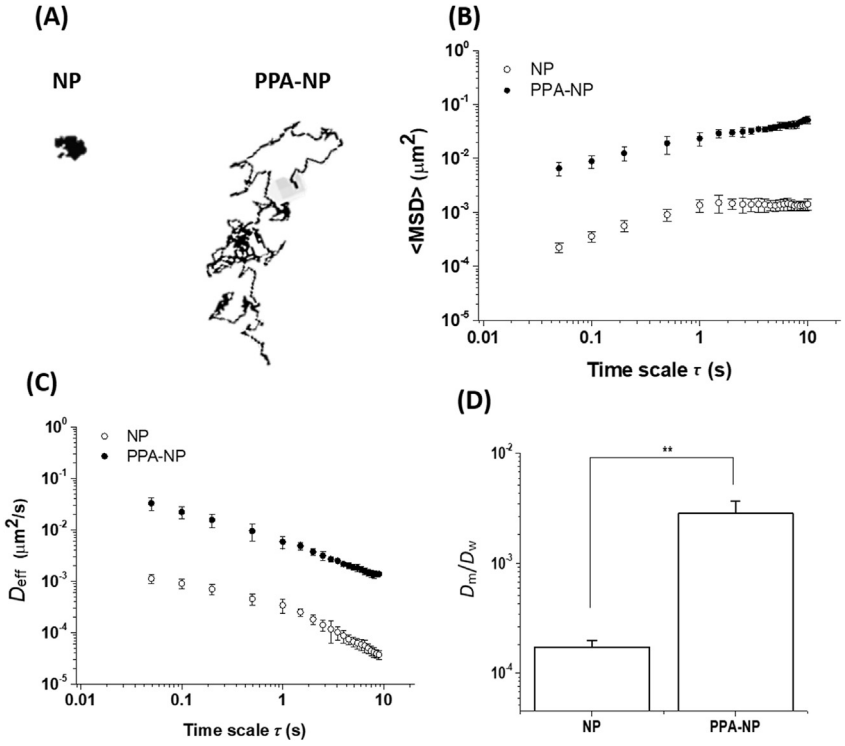

Figure 4 Transport of bare and PPA-coated nanoparticles in porcine intestinal mucus (A) Trajectories representative of 10 s movement of bare (NPs) and PPA-coated nanoparticles (PPA-NPs) (B) Ensemble-averaged geometric mean-squared displacements (<MSD>) as a function of time scale (C) Effective diffusivities ($<D_{eff}>$) as function of time scale. (d) Ratios of the average diffusion coefficient in mucus (D_m) compared to in water (D_w). Data represents three independent experiments, with $n \geq 110$ particles for each experiment ($^{**}P < 0.01$).

analyses were performed using a one-way ANOVA test followed by a Tukey−Kramer multi-comparison test. Significant differences between treatments are marked as follows: $^{*}P < 0.05$, $^{**}P < 0.01$, $^{***}P < 0.001$. For the lifespan assay, animal survival was plotted using Kaplan−Meier survival curves and analyzed by the log-rank test. Survival curves resulting in $P < 0.05$ relative to control were considered significantly different. All calculations were performed using StataSE v12 software (StataCorp, LLC, College Station, TX, USA), and the curves were plotted with the Origin 8 software (OriginLab Corp, Northampton, MA, USA).

3. Results

3.1. Synthesis and characterization of PEG-poly(anhydride) conjugate (PPA)

PPA conjugate was synthesized by forming ester linkages in a two steps reaction (Fig. 1A), which was confirmed by ^{1}H NMR and FT-IR. The ^{1}H NMR spectrum of the poly (anhydride), PEG and PPA conjugate are shown in Fig. 1B. The spectrum of the conjugate showed signals originated from both poly (anhydride) and PEG domains. Thus, the peaks at 3.2−3.5 ppm are characteristic of the tertiary carbons of the anhydride ring and $-OCH_3$ group of poly (anhydride), whereas the proton signals at 3.8−4.2 ppm correspond to a MeO−CH group. The incorporation of PEG was confirmed by the presence of peaks corresponding to ethylene (3.51 ppm) and hydroxyl groups (4.58 ppm). These signals were absent in the spectrum of poly (anhydride). The signal of the hydroxyl group at 4.58 ppm has been previously reported in PEGs in the presence of DMSO[26]. Finally, after conjugation, the signal corresponding to the hydrogen of the alpha-carbonyl (O═C−CH) emerged at 2−2.3 ppm, confirming the opening of anhydride groups.

FT-IR spectroscopy confirmed the formation of ester bond in PPA conjugate with the appearance of a new absorption band at 1735 cm^{-1}, which corresponds to carbonyl groups ν (–C═O) in the ester linkage (Fig. 1C). The bands at 1780 cm^{-1} and at 1853 cm^{-1} represent the anhydride carbonyl groups, which decreases after the incorporation of PEG due to the opened maleic anhydride group of poly (anhydride). Additionally, the appearance of characteristic PEG peaks corresponding to C−O−C stretching and C−H bending was observed at 1100, 1444 and 1349 cm^{-1} in PPA spectrum, suggesting successful synthesis of the conjugate.

Regarding elemental analysis, the increase in the C-to-O ratio for the PPA conjugate also confirms the incorporation of PEG chains in the structure of poly (anhydride). Furthermore, the lack of nitrogen allows us to infer that the conjugated PAA does not contain EDC residues (Table 1). Finally, the degree of substitution (DS) in the conjugate was calculated from the ^{1}H NMR spectra based on the ratio of the peak intensity of protons of the ethylene units (3.51 ppm) detected in the PAA conjugate and PEG spectra, respectively. This DS was calculated to be approximately 15.9%.

3.2. Characterization of nanoparticles

The preparative process of nanoparticles used in this study encompassed two different steps: (i) formation of insulin-loaded nanoparticles and (ii) coating of these nanoparticles with the PPA conjugate. The main physico-chemical characteristics of the

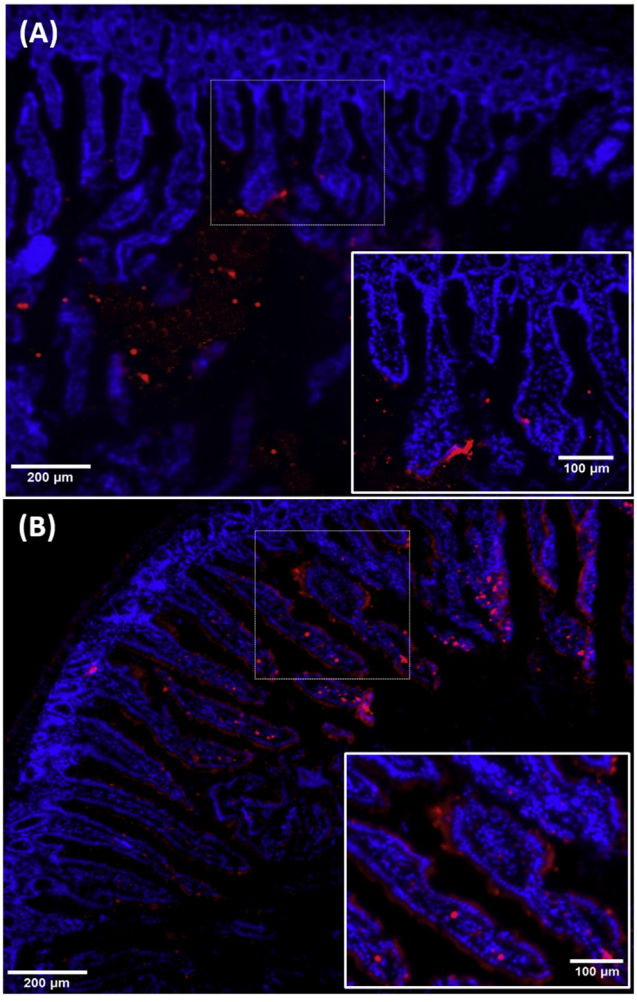

Figure 5 Fluorescence microscopic visualization of (A) bare and (B) PPA-coated nanoparticles in longitudinal sections of the ileum of rats. DAPI staining of nuclei appears as blue.

resulting nanoparticles are summarized in Table 2. The incorporation of insulin led to a significant increase of the mean size of the nanoparticles ($P < 0.001$) while the coating with PPA significantly decreased the negative zeta potential of the nanoparticles ($P < 0.001$). The insulin loading was calculated to be about 75 µg/mg nanoparticles, with an encapsulation efficiency of 78%. Under the experimental conditions evaluated, all the nanoparticle formulations displayed homogeneous characteristics with a PDI below 0.2 and yields close to 84%. For fluorescently labeled nanoparticles, the amount of Lumogen®F Red 305 incorporated into the nanoparticles was 0.73 ± 0.08 µg/mg.

The morphology of zein nanoparticles is shown in Fig. 2. The SEM micrograph displayed that both types of nanoparticles (bare and PPA-coated) were spherical in shape, but with apparent differences in their surface. NPs displayed a clearly smooth surface (Fig. 2A), while PPA-NPs showed a rough surface (Fig. 2B). The PPA coating led to larger and homogenous nanoparticles, which was consistent with the results obtained by spectroscopy (Table 2).

The surface hydrophobicity of nanoparticles was estimated by using the Rose Bengal method (Fig. 3). From these studies, the hydrophobicity of PPA-coated nanoparticles was calculated to be 2.3-times lower than for bare nanoparticles. Moreover, the incorporation of insulin into nanoparticles did not modify the surface hydrophobicity of the nanoparticles.

3.3. Evaluation of the mucus-penetrating properties of PPA-coated nanoparticles

In order to analyse the interaction of the PPA-coated nanoparticles with intestinal mucus, their diffusion in porcine intestinal mucus were assessed using multiple particle tracking (MPT). Fig. 4 shows a comparison of the transport of PPA-coated and bare nanoparticles in porcine intestinal mucus. Bare nanoparticles displayed confined particle trajectories, while PPA-coated nanoparticles exhibited Brownian-like trajectories that explored distances much wider than their diameters in the 10 s movies (Fig. 4A). The trajectories of particles were converted into geometric ensemble mean-squared displacements (MSD) as a function of time. Coating zein nanoparticles with the PPA-conjugate significantly increased the particle transport rates, as is evident by 20-fold higher MSD of PPA-NPs compared with bare nanoparticles at a 1 s time scale (Fig. 4B). The ensemble-average effective diffusivity (D_{eff}) for both types of nanoparticles decreased at short time scales, suggesting sub-diffusive transport in the mucus (Fig. 4C). However, the α value, which reflects the extent of impediment to particle motion ($\alpha = 1$ for free diffusion; $\alpha < 1$ reflects increased obstruction to particle movement) was significantly smaller for NPs than for PPA-NPs ($\alpha = 0.35$ *vs.* 0.86). Overall, NPs penetrated mucus with an average speed 5500-fold reduced compared to their theoretical speed in water (estimated by Stokes−Einstein). In contrast, PPA-NPs was slowed on average only 300-fold compared to rates in water. Further, when the insulin was loaded in PPA-NPs, similar results were observed to empty nanoparticles, indicating that insulin incorporation did not affect the diffusion properties of PPA-NPs (Fig. 4D).

The influence of PPA-coated on the capability of the resulting nanoparticles to reach the surface of the gut mucosa *in vivo* was also explored. Fig. 5 shows fluorescence microscopy images of ileum samples from the rats treated with Lumogen®F Red labeled nanoparticles 2 h post-administration. Bare nanoparticles displayed a localization mainly constrained to the mucus layer covering the intestinal epithelium, without any apparent presence between intestinal villi (Fig. 5A). On the contrary, the fluorescence associated with PPA-coated nanoparticles was observed mainly throughout and between the intestinal villi, so these carriers were able to penetrate the entire mucus barrier and distribute well on the epithelial surfaces (Fig. 5B). Regarding the aqueous suspension of Lumogen®F Red 305 (control formulation), large aggregates of the dye visualized in the lumen (data not shown).

3.4. In vivo evaluation of insulin-loaded nanoparticles in C. elegans

3.4.1. Nanoparticles intake

In order to confirm the route of exposure of PPA-NPs, worms were fed with Lumogen®F Red-labeled nanoparticles and observed by fluorescence microscopy. After 2 h of incubation, the fluorescently-labeled nanoparticles (PPA-NPs and NPs) were distributed throughout the intestinal tube of the worms from the pharynx to the rectum (Fig. 6A and B). These observations suggest that nanoparticles would enter in the worms *via* oral route during food intake. On the contrary, no presence of Lumogen F

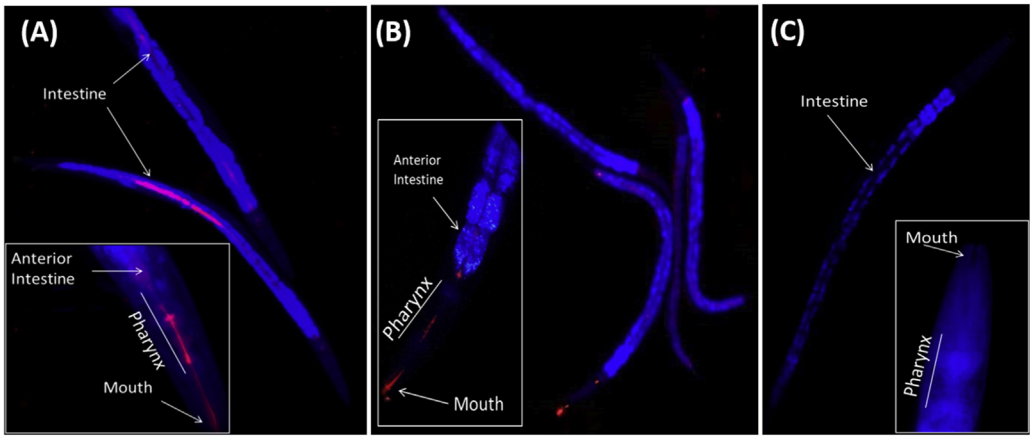

Figure 6 Fluorescence micrographs of representative *C. elegans* fed PPA-NPs (A) and NPs (B) containing Lumogen®F Red. As control, a suspension of Lumogen®F Red was employed (C). Blue signals represent autofluorescence of *C. elegans*. Red fluorescence represents Lumogen-loaded nanoparticles in the intestinal tract of worms 2 h after administration (zoom = 10 ×). In the white box, the mouth and the pharynx lumen are shown at 20 × magnification.

Red in the intestine of worms was observed when a suspension of the dye, used as control, was evaluated (Fig. 6C).

3.4.2. *Effect of insulin-loaded nanoparticles on glucose and fat content*

In order to study the effects of oral insulin (formulated in NPs or PPA-NPs) in *C. elegans*, the worms were grown in glucose-supplemented medium (50 mmol/L). The intracellular glucose content in nematodes was determined from whole-body extracts after a six days culture. The presence of glucose in the culture medium induced a significant increase in the intracellular content of saccharides with respect to the worms cultured in standard conditions (13.8 mmol/L *vs.* 5.5 mmol/L; $P < 0.001$). These increased levels of glucose were reduced by insulin treatment (Fig. 7A). Nanoencapsulated insulin showed a more significant reduction in glucose content (about 46%, $P < 0.01$) than free insulin (32%, $P < 0.05$). This decrease in the glucose content was also found to be associated with a significant reduction in the fat content of the worms, determined by Nile Red (Fig. 7B). Thus, the nematodes treated with I-PPA-NPs displayed a significantly lower amount of fat (25%) than the worms treated with bare nanoparticles (20%) or free insulin (11%) ($P < 0.01$).

3.4.3. *Effect of insulin-loaded nanoparticles on intracellular ROS and SOD activity*

Intracellular ROS levels were quantified in *C. elegans* grown in a medium with a high concentration of glucose and treated with insulin or insulin-loaded nanoparticles for six days. Consistent with previous reports, we found that glucose supplementation significantly induced the formation of intracellular ROS in worms[34,37]. Treatment with I-PPA-NPs decreased intracellular ROS by 44.3% ($P < 0.001$), while I-NPs and free insulin only reduced them by 37.7% and 21.8%, respectively ($P < 0.01$, Fig. 8A).

SOD is involved in ROS detoxification in *C. elegans*[34]. Thus, we evaluated whether the effect of insulin-loaded nanoparticles on intracellular ROS was related to the activity of this enzyme. Under our experimental conditions, untreated worms showed a decrease in SOD activity by 35.1% with respect to the worms cultured in standard conditions (data not shown). In contrast, worms treated with insulin (free or loaded in nanoparticles) restored SOD activity ($P < 0.01$, Fig. 8B). The activity of SOD in worms treated with free insulin was slightly higher than in worms treated with nanoencapsulated insulin (55.89% *vs.* 49.89%).

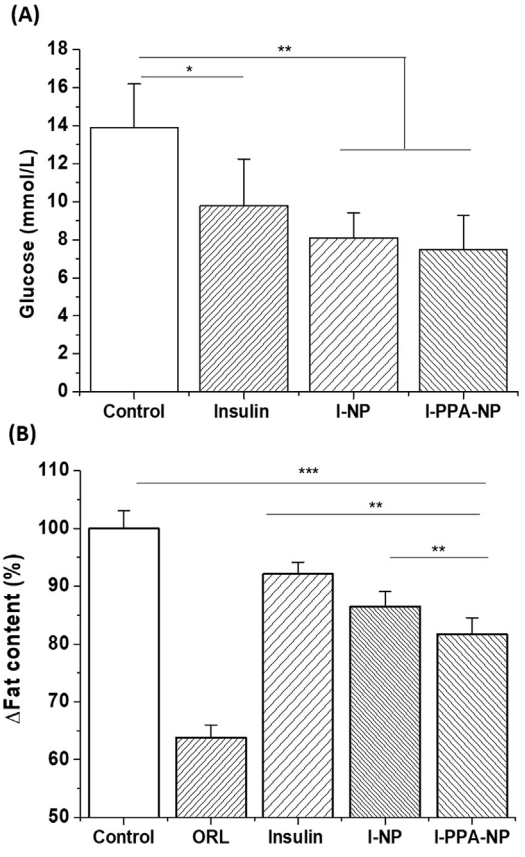

Figure 7 Effects of insulin (free or nanoencapsulated in bare or PPA-coated nanoparticles) on glucose (A) and fat content (B) of *C. elegans* cultivated under high glucose (50 mmol/L). Data represents three independent experiments with $n = 100$ worms for each experiment. *$P < 0.05$, **$P < 0.01$ and ***$P < 0.001$ for the indicated comparison. ORL: Orlistat.

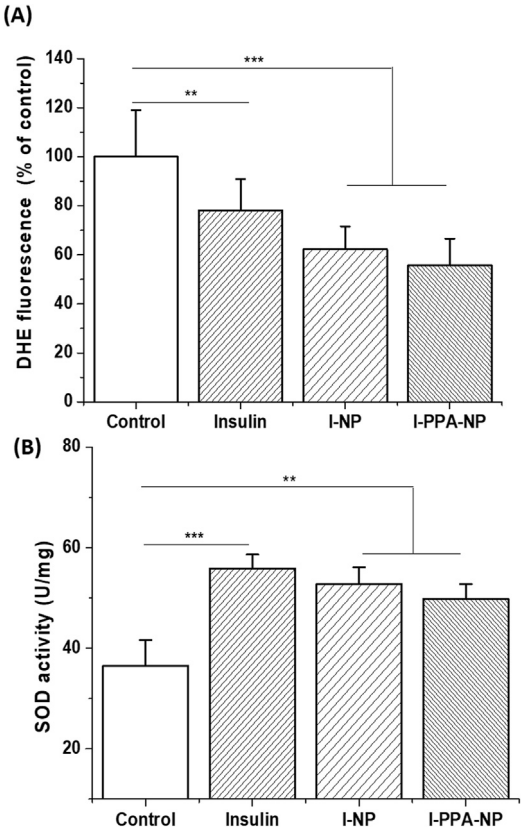

Figure 8 Effect of insulin (free or nanoencapsulated in bare and PPA-coated nanoparticles) on intracellular ROS levels (A) and SOD activity (B) of *C. elegans* growing high glucose concentrations (50 mmol/L). Data represents three independent experiments, with $n = 50$ worms for each experiment. *$P < 0.05$, **$P < 0.01$ and ***$P < 0.001$ for the indicated comparison.

3.4.4. *Effect of insulin-loaded nanoparticles on lifespan and ageing gene expression*

A high glucose diet has been associated with a reduced lifespan in *C. elegans*[37,41]. For this reason, the effect of insulin-loaded nanoparticles on the lifespan of *C. elegans* under high glucose conditions was evaluated (Fig. 9). As expected, the incorporation of high glucose levels in the diet of worms decreased the mean lifespan by 24.7% with respect to the worms cultured in standard conditions ($P < 0.001$; data not shown). On the contrary, when worms receiving the glucose-enriched diet were simultaneously treated with insulin (free or nanoencapsulated), their lifespan increased significantly ($P < 0.001$). The largest increase in the mean lifespan of worms was observed in worms treated with I-PPA-NPs. These worms displayed a mean lifespan of 10-days longer than untreated ones, while bare-NPs treatment only showed an increase of about 7 days (Fig. 9B).

In order to better characterize the molecular mechanisms responsible for this increase of lifespan, we assessed by qPCR expression changes in genes closely related to glucose metabolism, oxidative stress and longevity such as *daf-2*, *daf-16*, *skn-1* and *sod-3*[42]. To do this, synchronized wild-type L1 worms were treated with insulin (free or nanoencapsulated) for six days. The qRT-PCR results showed that insulin (free or nanoencapsulated) significantly down-regulated the expression of *daf-2* ($P < 0.05$), and up-regulated the expression of *daf-16* ($P < 0.01$), *sod-3* ($P < 0.05$) and *skn-1* ($P < 0.001$) (Fig. 10). In addition, the worms treated with I-PPA-NPs displayed a significantly higher expression of *skn-1* than worms treated with I-NPs or free insulin. *Daf-2* and *daf-16* expression changes were also significantly different in the worms treated with I-PPA-NPs than with free insulin.

4. Discussion

In this work, zein nanoparticles coated with a shield containing PEG 2000 were employed as oral nanocarriers for insulin. The synthesis of PEG-poly (anhydride) conjugate (PPA) was performed by Steglich esterification reaction under water-free and oxygen-free conditions and confirmed by ^{1}H NMR and FT-IR (Fig. 1). The substitution degree was calculated to be 15.9% (about 158.5 μg of PEG per mg conjugate).

The idea of using this type of conjugate was that the hydrophobic segments of the conjugate (*i.e.*, methylvinylether groups) would interact with the surface of the nanoparticles, leaving hydrophilic PEG chains protruding from the surface of the particle in contact with the dispersing aqueous medium. This mechanism has been previously demonstrated to explain the adsorption of amphiphilic copolymers onto hydrophobic nanoparticles[43,44]. In

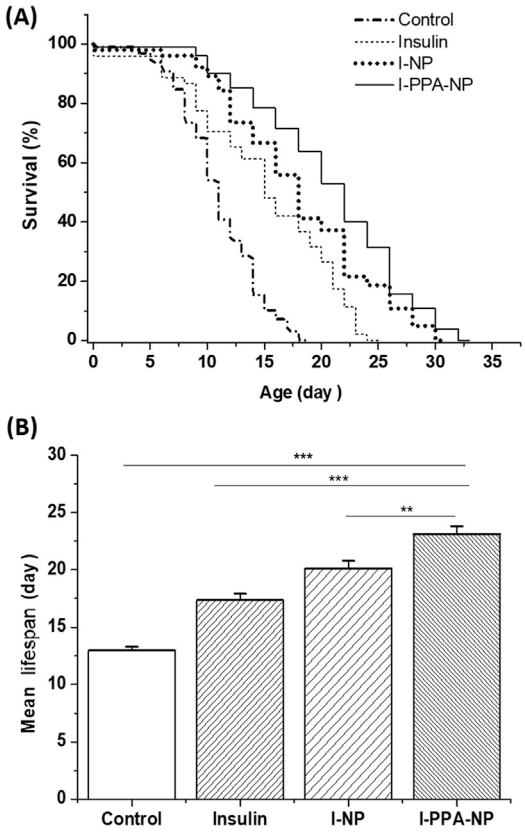

Figure 9 Effect of insulin (free or encapsulated in bare or PPA-coated nanoparticles) on lifespan in *C. elegans* grown under high glucose conditions (50 mmol/L) (A) Kaplan−Meier plots of the fraction of living *C. elegans*. Data are displayed as the average curves of three independent experiments, with $n = 100$ worms for each experiment (B) The mean lifespan of wild-type nematodes was calculated from the survival curves shown in (A). The difference between groups was calculated using the log-rank test. **$P < 0.01$, ***$P < 0.001$ for the indicated comparison.

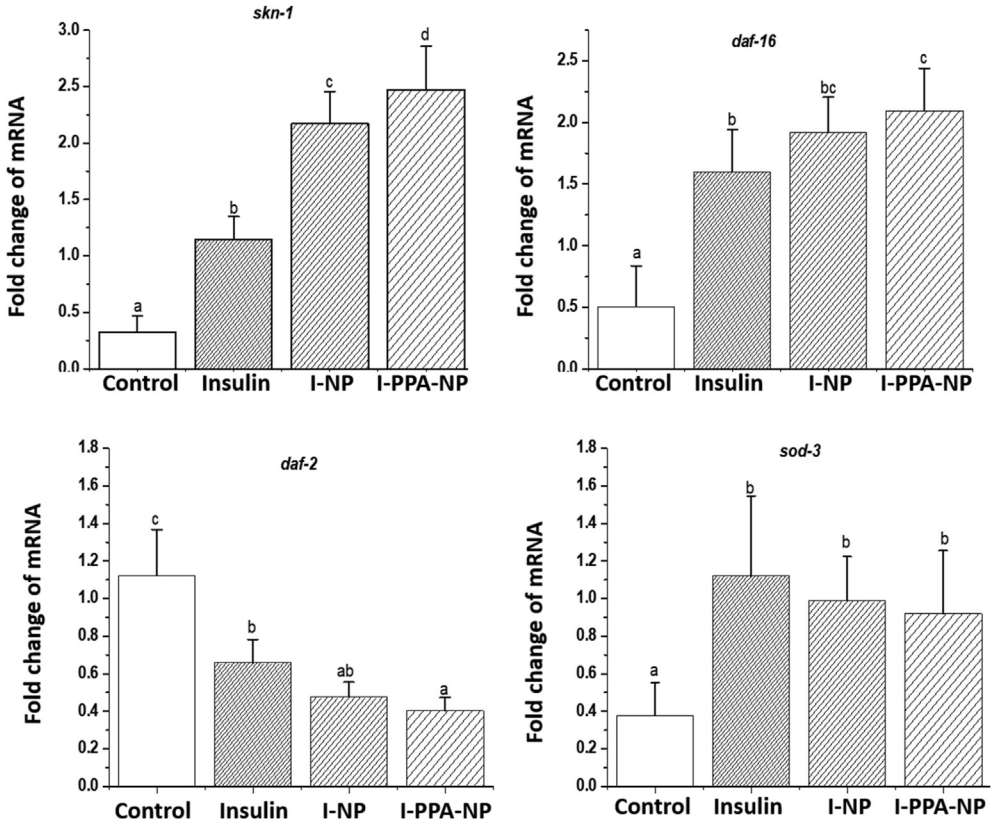

Figure 10 Effect of insulin (free or encapsulated in bare or PPA-coated nanoparticles) on the gene expression in *C. elegans* grown under high glucose conditions (50 mmol/L). The mRNA expression levels of *skn-1*, *daf-16*, *daf-2* and *sod-3* were determined by qRT-PCR and normalized to *pmp-1* expression. Different letters on bars indicate statistical differences among groups ($P < 0.05$, mean ± SD, $n = 4$).

our case, the coating with PPA conjugate modified the surface of zein nanoparticles, reducing their negative surface charge (from −45 to −32 mV, Table 2) and hydrophobicity (2.5-fold lower, Fig. 3). Furthermore, these nanoparticles (PPA-NPs) showed a rough surface by SEM in contrast to the smooth appearance of bare nanoparticles (Fig. 2), probably attributable to the adsorption of the PPA conjugate on the surface. The MPT studies also showed that PPA-NPs exhibited not only much less obstructed Brownian motion in mucus compared to NPs, but also 20-fold improved diffusion properties in porcine intestinal mucus (Fig. 4). This greater diffusivity of PPA-NPs in the mucus was corroborated in the biodistribution study with fluorescently labelled nanoparticles. As expected, bare nanoparticles were enriched in the mucus layer covering the epithelium, in which they were mostly aggregated and trapped within the mucus, away from the absorptive epithelium (Fig. 5B). On the contrary, the mucus-permeating properties of PPA-NPs facilitated their arrival (to a large extent) to intestinal epithelium (Fig. 5B). These results are in agreement with previous studies that demonstrate the ability of PEGylated nanoparticles to diffuse unimpeded through the mucus layer[31,45]. Another interesting aspect to note is that the PPA-NPs were able to quickly reach specific intestinal regions favorable for insulin absorption (*i.e.*, ileum). This region, together with the jejunum, has been reported to have greater permeability than other segments of the intestinal tract[46].

Regarding the encapsulation of insulin, the amount of hormone loaded in nanoparticles was not affected by the coating with the PPA conjugate. On the contrary, the incorporation of insulin into nanoparticles caused a significant increase in the mean size of the nanoparticles (Table 2), in any case, this increase did not modify the surface hydrophobicity and diffusion properties observed in the empty PPA-NPs (Figs. 3 and 4D).

The *in vivo* efficacy of insulin-loaded nanoparticles was evaluated in the *C. elegans* model under high glucose conditions, comparable with the blood glucose levels observed in diabetic patients[32,47]. The evaluation of the fate of nanoparticles within *C. elegans* was achieved thanks to the transparency of the worm and the use of fluorescently-labelled nanoparticles. The nanoparticles were localized only in the intestine tract of the worms (Fig. 6), indicating oral route as the exclusive portal of entry. Thus, the results found to correspond to the behaviour of the nanoparticles within the GIT of the worm.

The effects of a high-glucose diet in *C. elegans* has been shown to cause toxicity, which results in lipid accumulation[48], increasing levels of reactive oxygen species (ROS)[49], and a significant reduction in lifespan[41]. We found that insulin treatment protected from damage by glucose toxicity by extending the lifespan of worms (Fig. 9), reducing ROS levels (Fig. 8) and fat accumulation (Fig. 7). These results are consistent with a previous study that demonstrated the protective effect of human insulin against the damage induced by a high glucose diet[34]. It was suggested that the effect would be mediated by a DAF-2/insulin receptor and DAF-16/FOXO-dependent pathways, leading to glucose-lowering and activation of detoxification systems such as iron/manganese SOD (SOD-3) and glyoxalase-1[34]. In fact, we have found that insulin treatment significantly reduces glucose concentration (Fig. 7B), ROS levels (Fig. 8A), recovery of SOD activity (Fig. 8B) and promotes *daf-16* expression (Fig. 10). Additionally, insulin

treatment reduces fat accumulation (Fig. 7A) and promotes *skn-1* expression (Fig. 10).

Reduction of the insulin/IGF-1 signalling (IIS) pathway has been related to improved stress resistance and longevity in many organisms[18]. It has been reported that when IIS is reduced, lifespan is doubles, and this extension of lifespan requires DAF-16, a member of the FOXO-family of transcription factors[50,51]. Consistent with this, we found that insulin treatment increased the mean lifespan in the worms, also showing an up-regulation of *daf-16* and a down-regulation of *daf-2*. In particular, the worms treated with I-PPA-NPs showed a mean lifespan 2-times higher than the untreated ones, accompanied by a higher *daf-16* expression. These findings agree with the fact that human insulin binds to the *C. elegans* insulin receptor DAF-2 (which has high homology to the mammalian receptor) in an antagonistic manner[52], thus inactivating DAF-2 signalling. The inhibition of DAF-2 leads to decreased activities in IIS protein kinases, including AKT-1/-2. This effect reduces the phosphorylation of DAF-16 and SKN-1 transcription factors, thereby promoting their activation *via* nuclear localization[53]. These results confirm the interaction of insulin released from nanoparticles with the DAF-2/insulin receptor.

On the other hand, a reduced IIS also causes a restriction in glucose metabolism, leading to an increase in mitochondrial activity and a better stress response to ROS through SKN-1[54]. SKN-1, an ortholog of mammalian Nrf-2, contributes to the increased stress tolerance and longevity resulting from the reduction of IIS[37]. SKN-1 also regulates other processes such as immune defense and lipid metabolism. A previous study found that a *skn-1* gain-of-function mutation protects worms against increased lipid storage when fed a high glucose diet[55]. Treatment with insulin-loaded nanoparticles markedly increased *skn-1* expression (Fig. 10). Thus, the reduction in fat storage observed in worms can, at least in part, be attributed to this up-regulation of *skn*-1 by insulin treatment. Interestingly, there is a relationship between the up-regulation of *skn*-1 by the different treatments (Fig. 10) and its effect on fat accumulation in worms (Fig. 7B).

The effect of insulin on lifespan, ROS levels and fat accumulation increased with its encapsulation into nanoparticles. This could be associated with the protection of insulin against the enzymatic degradation in the intestine of worms, where several digestive enzymes are secreted, mostly proteases[20]. Indeed, the treatment with insulin-loaded in PPA-NPs showed a greater protective effect on glucose toxicity than bare nanoparticles. Given that the intestinal epithelium of *C. elegans* is protected by a peritrophic-like dense layer, similar to the mucus layer in the human intestinal cell[19], the protective effect observed in I-PPA-NPs would be related to their high capability to diffuse in mucus, facilitating its arrival to the absorptive epithelium and, thus, the release of insulin and its absorption.

5. Conclusions

In summary, the coating of zein-based nanoparticles with a PEG-Gantrez®AN conjugate resulted in mucus-permeating nanocarriers capable of overcoming the mucus barrier, facilitating their arrival to the intestinal epithelium. Interestingly, the incorporation of insulin into these nanoparticles did not modify their surface hydrophobicity and diffusion properties. In the *C. elegans* model, these insulin-loaded nanoparticles (PPA-NPs) induced a significant reduction in the formation of ROS and the fat accumulated in the body. Besides, I-PPA-NPs increased the lifespan of worms by interaction with at least DAF-2 receptor. These results are encouraging, and more experiments would be necessary to confirm the pharmacological effect of this strategy in an *in vivo* mammal model. In addition, these results suggest that *C. elegans* offers promising characteristics and valuable tools for evaluating oral insulin delivery systems before moving to more complex model organisms.

Acknowledgments

The first author was supported by Postdoctoral Fellowship from the National Council for Science and Technology of Mexico (CONACyT, Grant No. 291231, Mexico).

Author contributions

Juan M. Irache, Carlos J. González-Navarro and José L. Vizmanos designed the research. Ana L. Martínez-López carried out the experiments and performed data analysis. Paula Aranaz participated part of the experiments. Juan M. Irache, Carlos J. González-Navarro and José L. Vizmanos provided experimental drugs and quality control. Ana L. Martínez-López wrote the manuscript. Juan M. Irache, Carlos J. González-Navarro, José L. Vizmanos and Paula Aranaz revised and edited the manuscript. All of the authors have read and approved the final manuscript.

Conflicts of interest

The authors have no conflicts of interest to declare.

References

1. Muheem A, Shakeel F, Jahangir MA, Anwar M, Mallick N, Jain GK, et al. A review on the strategies for oral delivery of proteins and peptides and their clinical perspectives. *Saudi Pharmaceut J* 2016;**24**:413−28.
2. Cao SJ, Xu S, Wang HM, Ling Y, Dong J, Xia RD, et al. Nanoparticles: oral delivery for protein and peptide drugs. *AAPS PharmSciTech* 2019;**20**:1−11.
3. Han Y, Gao Z, Chen L, Kang L, Huang W, Jin M, et al. Multifunctional oral delivery systems for enhanced bioavailability of therapeutic peptides/proteins. *Acta Pharm Sin B* 2019;**9**:902−22.
4. Perry SL, McClements DJ. Recent advances in encapsulation, protection, and oral delivery of bioactive proteins and peptides using colloidal systems. *Molecules* 2020;**25**:1−26.
5. Al-Remawi M, Elsayed A, Maghrabi I, Hamaidi M, Jaber N. Chitosan/lecithin liposomal nanovesicles as an oral insulin delivery system. *Pharmaceut Dev Technol* 2017;**22**:390−8.
6. Zhang X, Qi J, Lu Y, He W, Li X, Wu W. Biotinylated liposomes as potential carriers for the oral delivery of insulin. *Nanomedicine* 2014;**10**:167−76.
7. Lundquist P, Artursson P. Oral absorption of peptides and nanoparticles across the human intestine: opportunities, limitations and studies in human tissues. *Adv Drug Deliv Rev* 2016;**106**:256−76.
8. McClements DJ. Encapsulation, protection, and delivery of bioactive proteins and peptides using nanoparticle and microparticle systems: a review. *Adv Colloid Interface Sci* 2018;**253**:1−22.
9. Wong CY, Martinez J, Dass CR. Oral delivery of insulin for treatment of diabetes: status quo, challenges and opportunities. *J Pharm Pharmacol* 2016;**68**:1093−108.

10. Macedo A, Filipe P, Thomé NG, Vieira J, Oliveira C, Teodósio C, et al. A brief overview of the oral delivery of insulin as an alternative to the parenteral delivery. *Curr Mol Med* 2020;**20**:134−43.
11. Ensign LM, Cone R, Hanes J. Oral drug delivery with polymeric nanoparticles: the gastrointestinal mucus barriers. *Adv Drug Deliv Rev* 2012;**64**:557−70.
12. Pereira De Sousa I, Moser T, Steiner C, Fichtl B, Bernkop-Schnürch A. Insulin loaded mucus permeating nanoparticles: addressing the surface characteristics as feature to improve mucus permeation. *Int J Pharm* 2016;**500**:236−44.
13. Bourganis V, Karamanidou T, Samaridou E, Karidi K, Kammona O, Kiparissides C. On the synthesis of mucus permeating nanocarriers. *Eur J Pharm Biopharm* 2015;**97**:239−49.
14. Inchaurraga L, Martínez-López AL, Cattoz B, Gri PC, Wilcox M, Pearson P, et al. The effect of thiamine-coating nanoparticles on their biodistribution and fate following oral administration. *Eur J Pharmaceut Sci* 2019;**128**:81−90.
15. Gonzalez-Moragas L, Roig A, Laromaine A. *C. elegans* as a tool for *in vivo* nanoparticle assessment. *Adv Colloid Interface Sci* 2015;**219**:10−26.
16. Moraes BKS, Vieira SM, Salgueiro WG, Michels LR, Colomé LM, Avila DS, et al. Clozapine-loaded polysorbate-coated polymeric nanocapsules: physico-chemical characterization and toxicity evaluation in *Caenorhabditis elegans* model. *J Nanosci Nanotechnol* 2016;**16**:1257−64.
17. Kaletta T, Hengartner MO. Finding function in novel targets: *C. elegans* as a model organism. *Nat Rev Drug Discov* 2006;**5**:387−99.
18. Kenyon C. The plasticity of aging: insights from long-lived mutants. *Cell* 2005;**120**:449−60.
19. Everman JL, Ziaie NR, Bechler J, Bermudez LE. Establishing *Caenorhabditis elegans* as a model for *Mycobacterium avium* subspecies hominissuis infection and intestinal colonization. *Biol Open* 2015;**4**:1330−5.
20. Dimov I, Maduro MF. The *C. elegans* intestine: organogenesis, digestion, and physiology. *Cell Tissue Res* 2019;**377**:383−96.
21. Laughlin ST, Bertozzi CR. *In vivo* imaging of *Caenorhabditis elegans* glycans. *ACS Chem Biol* 2009;**4**:1068−72.
22. Martínez-López AL, Pangua C, Reboredo C, Campión R, Morales-Gracia J, Irache JM. Protein-based nanoparticles for drug delivery purposes. *Int J Pharm* 2020;**581**:119289.
23. Peñalva R, Esparza I, González-Navarro CJ, Quincoces G, Peñuelas I, Irache JM. Zein nanoparticles for oral folic acid delivery. *J Drug Deliv Sci Technol* 2015;**30**:450−7.
24. Inchaurraga L, Martínez-López AL, Martin-Arbella N, Irache JM. Zein-based nanoparticles for the oral delivery of insulin. *Drug Deliv Transl Res* 2020;**10**:1601−11.
25. Lucio D, Martínez-Ohárriz MC, Gu Z, He Y, Aranaz P, Vizmanos JL, et al. Cyclodextrin-grafted poly(anhydride) nanoparticles for oral glibenclamide administration. *In vivo* evaluation using *C. elegans*. *Int J Pharm* 2018;**547**:97−105.
26. Yoncheva K, Lizarraga E, Irache JM. Pegylated nanoparticles based on poly(methyl vinyl ether-*co*-maleic anhydride): preparation and evaluation of their bioadhesive properties. *Eur J Pharmaceut Sci* 2005;**24**:411−9.
27. Doktorovova S, Shegokar R, Martins-Lopes P, Silva AM, Lopes CM, Müller RH, et al. Modified Rose Bengal assay for surface hydrophobicity evaluation of cationic solid lipid nanoparticles (cSLN). *Eur J Pharmaceut Sci* 2012;**45**:606−12.
28. Abdulkarim M, Agulló N, Cattoz B, Griffiths P, Bernkop-Schnürch A, Borros SG, et al. Nanoparticle diffusion within intestinal mucus: three-dimensional response analysis dissecting the impact of particle surface charge, size and heterogeneity across polyelectrolyte, pegylated and viral particles. *Eur J Pharm Biopharm* 2015;**97**:230−8.
29. Inchaurraga L, Martínez-López AL, Abdulkarim M, Gumbleton M, Quincoces G, Peñuelas I, et al. Modulation of the fate of zein nanoparticles by their coating with a Gantrez® AN-thiamine polymer conjugate. *Int J Pharm X* 2019;**1**:100006.
30. Schindelin J, Arganda-Carreras I, Frise E, Kaynig V, Longair M, Pietzsch T, et al. Fiji: an open-source platform for biological-image analysis. *Nat Methods* 2012;**9**:676−82.
31. Inchaurraga L, Martín-Arbella N, Zabaleta V, Quincoces G, Peñuelas I, Irache JM. *In vivo* study of the mucus-permeating properties of PEG-coated nanoparticles following oral administration. *Eur J Pharm Biopharm* 2015;**97**:280−9.
32. Brenner S. The genetics of *Caenorabditis elegans*. *Genetics* 1974;**77**:71−94.
33. Martorell P, Llopis S, González N, Montón F, Ortiz P, Genovés S, et al. *Caenorhabditis elegans* as a model to study the effectiveness and metabolic targets of dietary supplements used for obesity treatment: the specific case of a conjugated linoleic acid mixture (Tonalin). *J Agric Food Chem* 2012;**60**:11071−9.
34. Mendler M, Schlotterer A, Ibrahim Y, Kukudov G, Fleming T, Bierhaus A, et al. *daf-16*/FOXO and *glod-4*/glyoxalase-1 are required for the life-prolonging effect of human insulin under high glucose conditions in *Caenorhabditis elegans*. *Diabetologia* 2014;**58**:393−401.
35. Navarro-Herrera D, Aranaz P, Eder-Azanza L, Zabala M, Hurtado C, Romo-Hualde A, et al. Dihomo-gamma-linolenic acid induces fat loss in: *C. elegans* in an omega-3-independent manner by promoting peroxisomal fatty acid β-oxidation. *Food Funct* 2018;**9**:1621−37.
36. Wang Z, Ma X, Li J, Cui X. Peptides from sesame cake extend healthspan of *Caenorhabditis elegans via* upregulation of *skn-1* and inhibition of intracellular ROS levels. *Exp Gerontol* 2016;**82**:139−49.
37. Schlotterer A, Kukudov G, Bozorgmehr F, Hutter H, Du X, Oikonomou D, et al. *C. elegans* as model for the study of high glucose-mediated life span reduction. *Diabetes* 2009;**58**:2450−6.
38. Aranaz P, Navarro-Herrera D, Romo-Hualde A, Zabala M, López-Yoldi M, González-Ferrero C, et al. Broccoli extract improves high fat diet-induced obesity, hepatic steatosis and glucose intolerance in Wistar rats. *J Funct Foods* 2019;**59**:319−28.
39. Wu H, Taki FA, Zhang Y, Dobbins DL, Pan X. Evaluation and identification of reliable reference genes for toxicological study in *Caenorhabditis elegans*. *Mol Biol Rep* 2014;**41**:3445−55.
40. Livak KJ, Schmittgen TD. Analysis of relative gene expression data using real-time quantitative PCR and the $2^{-\Delta\Delta CT}$ method. *Methods* 2001;**25**:402−8.
41. Lee SJ, Murphy CT, Kenyon C. Glucose Shortens the Life Span of *C. elegans* by downregulating DAF-16/FOXO activity and aquaporin gene expression. *Cell Metabol* 2009;**10**:379−91.
42. Tullet JMA, Hertweck M, An JH, Baker J, Hwang JY, Liu S, et al. Direct inhibition of the longevity-promoting factor SKN-1 by insulin-like signaling in *C. elegans*. *Cell* 2008;**132**:1025−38.
43. Schubert S, Delaney Jr JT, Schubert US. Nanoprecipitation and nanoformulation of polymers: from history to powerful possibilities beyond poly(lactic acid). *Soft Matter* 2011;**7**:1581−8.
44. Li YP, Pei YY, Zhang XY, Gu ZH, Zhou ZH, Yuan WF, et al. PEGylated PLGA nanoparticles as protein carriers: synthesis, preparation and biodistribution in rats. *J Control Release* 2001;**71**:203−11.
45. Mura S, Hillaireau H, Nicolas J, Kerdine-Römer S, Le Droumaguet B, Deloménie C, et al. Biodegradable nanoparticles meet the bronchial airway barrier: how surface properties affect their interaction with mucus and epithelial cells. *Biomacromolecules* 2011;**12**:4136−43.
46. Agarwal V, Nazzal S, Reddy IK, Khan MA. Transport studies of insulin across rat jejunum in the presence of chicken and duck ovomucoids. *J Pharm Pharmacol* 2001;**53**:1131−8.
47. Zhu G, Yin F, Wang L, Wei W, Jiang L, Qin J. Modeling type 2 diabetes-like hyperglycemia in *C. elegans* on a microdevice. *Integr Biol (Cam)* 2016;**8**:30−8.
48. Lu Z, Qiu Z. High glucose concentration restricts fat consumption in *Caenorhabditis elegans*. *Int J Clin Exp Med* 2017;**10**:10554−9.
49. Schulz TJ, Zarse K, Voigt A, Urban N, Birringer M, Ristow M. Glucose restriction extends *Caenorhabditis elegans* life span by

inducing mitochondrial respiration and increasing oxidative stress. *Cell Metabol* 2007;**6**:280−93.
50. Kimura KD, Tissenbaum HA, Liu Y, Ruvkun G. daf-2, an insulin receptor-like gene that regulates longevity and diapause in *Caenorhabditis elegans*. *Science* 1997;**277**:942−6.
51. Sun X, Chen W-D, Wang Y-D. DAF-16/FOXO Transcription factor in aging and longevity. *Front Pharmacol* 2017;**8**:548.
52. Pierce SB, Costa M, Wisotzkey R, Devadhar S, Homburger SA, Buchman AR, et al. Regulation of DAF-2 receptor signaling by human insulin and ins-1, a member of the unusually large and diverse *C. elegans* insulin gene family. *Genes Dev* 2001;**15**:672−86.
53. Tullet JMA, Green JW, Au C, Benedetto A, Thompson MA, Clark E, et al. The *SKN-1/Nrf 2* transcription factor can protect against oxidative stress and increase lifespan in *C. elegans* by distinct mechanisms. *Aging Cell* 2017;**16**:1191−4.
54. Zarse K, Schmeisser S, Groth M, Priebe S, Beuster G, Kuhlow D, et al. Impaired insulin/IGF1 signaling extends life span by promoting mitochondrial L-proline catabolism to induce a transient ROS signal. *Cell Metabol* 2012;**15**:451−65.
55. Pang S, Lynn DA, Lo JY, Paek J, Curran SP. SKN-1 and Nrf 2 couples proline catabolism with lipid metabolism during nutrient deprivation. *Nat Commun* 2014;**5**:5048.